3-Hydroxyisobutyrate Dehydrogenase Is Involved in Both, Valine and Isoleucine Degradation in *Arabidopsis thaliana*[1][OPEN]

Peter Schertl, Lennart Danne, and Hans-Peter Braun[2]

Institut für Pflanzengenetik, Leibniz Universität Hannover, 30419 Hannover, Germany

ORCID ID: 0000-0002-4459-9727 (H.-P.B.).

In plants, amino acid catabolism is especially relevant in metabolic stress situations (e.g. limited carbohydrate availability during extended darkness). Under these conditions, amino acids are used as alternative substrates for respiration. Complete oxidation of the branched-chain amino acids (BCAAs) leucine, isoleucine (Ile), and valine (Val) in the mitochondria efficiently allows the formation of ATP by oxidative phosphorylation. However, the metabolic pathways for BCAA breakdown are largely unknown so far in plants. A systematic search for Arabidopsis (*Arabidopsis thaliana*) genes encoding proteins resembling enzymes involved in BCAA catabolism in animals, fungi, and bacteria as well as proteomic analyses of mitochondrial fractions from Arabidopsis allowed the identification of a putative 3-hydroxyisobutyrate dehydrogenase, AtHDH1 (At4g20930), involved in Val degradation. Systematic substrate screening analyses revealed that the protein uses 3-hydroxyisobutyrate but additionally 3-hydroxypropionate as substrates. This points to a role of the enzyme not only in Val but possibly also in Ile metabolism. At4g20930 knockdown plants were characterized to test this conclusion. Root toxicity assays revealed increased root growth inhibition of the mutants if cultivated in the presence of Val or Ile but not in the presence of leucine. We conclude that AtHDH1 has a dual role in BCAA metabolism in plants.

Plants can synthesize all 20 proteinogenic amino acids. Their carbon skeletons and amino groups directly or indirectly derive from photosynthesis. Besides amino acid biosynthesis, plants also can break down all 20 amino acids. Amino acid catabolism is especially relevant in the context of germination (the conversion of storage proteins into carbohydrates), senescence (the recycling of energy-rich compounds), and in the context of stress reactions (Hildebrandt et al., 2015). The synthesis of some amino acids is massively induced upon drought and salt stress, most of all proline, because they can serve as compatible osmolytes (Szabados and Savouré, 2010). Upon stress release, these amino acids are rapidly degraded. Furthermore, amino acid catabolism is essential for respiration in low-light conditions or extended darkness. Upon light shortage, the availability of carbohydrates for respiration is limited, and amino acids can be used as alternative respiratory substrates (Araújo et al., 2011). Amino acid catabolism mainly takes place in the mitochondria of plants, but most enzymatic reactions so far have not been characterized (Hildebrandt et al., 2015). They may or may not resemble reactions taking place in mammalian cells, which have been investigated extensively (Harper et al., 1984).

The branched-chain amino acids (BCAAs) Leu, Ile, and Val have aliphatic and comparably short side chains. Their concentrations increase under various stress conditions (Zhao et al., 1998; Joshi et al., 2010). The complete oxidation of BCAAs in the mitochondria allows the generation of high amounts of ATP (Hildebrandt et al., 2015). Indeed, it has been shown that the degradation pathways for BCAAs are up-regulated in extended darkness (Däschner et al., 2001; Ishizaki et al., 2005; Araújo et al., 2010; Binder, 2010). The BCAA catabolic pathways are especially complicated and, so far, only fragmentarily understood in plants.

The first two steps in the degradation of Val, Ile, and Leu are identical (see Fig. 7, which summarizes the known and putative steps of BCAA catabolism in plants). After an initial transamination reaction, the BCAAs are decarboxylated. Several transaminases that use BCAAs as substrates have been identified in plants. As a result, branched-chain 2-oxoacids are produced (Angelovici et al., 2013). The decarboxylation of the BCAAs is carried out by the branched-chain α-ketoacid dehydrogenase

complex (BCKDH), which is a very large complex and consists of multiple copies of the three enzymes E1, E2, and E3 (Mooney et al., 2002). The third enzyme in the degradation of Leu is the isovaleryl-CoA dehydrogenase (IVDH). This enzyme most likely also is involved in the parallel step of Val and Ile breakdown pathways. IVDH is a flavoenzyme that transfers electrons to the Electron Transfer Flavoprotein (ETF; Däschner et al., 2001; Araújo et al., 2010). The fourth biochemical step, a carboxylation reaction, is only known for Leu catabolism (Alban et al., 1993; Anderson et al., 1998). Starting from this point, further steps in the degradation of the three BCAAs are not known in plants. Only putative enzymes showing some degree of sequence similarity to already identified and characterized mammalian and bacterial enzymes have been reported (Hildebrandt et al., 2015). Most likely, an enoyl-CoA hydratase is involved in converting methyl-glutaconyl-CoA coming from Leu as well as 2-methylbutanoyl-CoA and 2-methylpropanoyl-CoA coming from Ile and Val catabolism, respectively. From this step, the three degradation pathways are predicted to differ. The final reaction in Leu catabolism is the conversion of 3-hydroxymethylglutaryl-CoA to acetyl-CoA and acetoacetate. In Ile catabolism, probably a 3-hydroxyacyl-CoA dehydrogenase and a 3-ketoacyl-CoA thiolase are involved in the formation of acetyl-CoA. The terminal steps of Val catabolism seem to be most complex. Probably, 3-hydroxyisobutyrate is formed from 3-hydroxyisobutyryl-CoA by a hydrolyzation reaction. Next, an oxidation takes place that is catalyzed by 3-hydroxyisobutyrate dehydrogenase. This step is special in the degradation of BCAAs because 3-hydroxyisobutyrate is not coupled to CoA. Different mammalian as well as bacterial 3-hydroxyisobutyrate dehydrogenases have been characterized in detail (Rougraff et al., 1988; Hawes et al., 1995, 1996; Chowdhury et al., 2003; Murín et al., 2008; Lee et al., 2014; Park et al., 2016). In contrast, this enzyme has not been characterized in plants so far. The product of the reaction catalyzed by 3-hydroxyisobutyrate dehydrogenase is methylmalonate semialdehyde. A final decarboxylase of the Val catabolic pathway catalyzes the conversion of methylmalonate semialdehyde into propionyl-CoA. The breakdown of propionyl-CoA in plants results in acetyl-CoA. It has been suggested that at least parts of this pathway in plants are carried out by the same set of enzymes that convert 3-hydroxyisobutyryl-CoA to propionyl-CoA (Hildebrandt et al., 2015).

We here describe the identification and characterization of a 3-hydroxyisobutyrate dehydrogenase (AtHDH1) in Arabidopsis (*Arabidopsis thaliana*). The enzyme was recombinantly expressed in *Escherichia coli* and affinity purified. The native state and the enzyme properties of AtHDH1 were determined. Besides 3-hydroxyisobutyrate, AtHDH1 converts 3-hydroxypropionate and methyl-3-hydroxy-2-methylpropionate, as revealed by systematic substrate screening analyses. This points to a role of AtHDH1 not only in Val but also in Ile metabolism. Root toxicity assays using AtHDH1 knockdown plants were employed to evaluate the physiological role of AtHDH1 in plants. The results indicate a role of AtHDH1 in both Val and Ile catabolism but not in the breakdown of Leu.

RESULTS

Identification of a Putative 3-Hydroxyisobutyrate Dehydrogenase from Arabidopsis

To better understand amino acid degradation in plants, the Arabidopsis genome sequence was systematically searched for genes encoding proteins similar to known enzymes involved in amino acid catabolism in animals, fungi, or bacteria (Hildebrandt et al., 2015). Furthermore, genes encoding mitochondrial dehydrogenases were systematically searched based on sequence comparisons (Schertl and Braun, 2014). Finally, shotgun proteome data sets of mitochondrial fractions from Arabidopsis were searched for putative enzymes involved in amino acid catabolism (Schertl, 2015). One identified gene encodes a 6-phosphogluconate dehydrogenase family protein (annotation by TAIR; accession no. At4g20930). Besides resembling 6-phosphogluconate dehydrogenase family proteins, the protein was found to exhibit sequence similarity to mammalian 3-hydroxyisobutyrate dehydrogenases (HDH; Supplemental Fig. S1). The protein At4g20930 was identified previously in a mitochondrial fraction of Arabidopsis in the course of a 2D gel-based proteome project (Taylor et al., 2011; Supplemental Fig. S2). It has an apparent molecular mass of 34 kD. Furthermore, At4g20930 has been identified in a mitochondrial fraction of Arabidopsis by a complexome-profiling approach (Senkler et al., 2017).

Recombinant Expression and Purification of At4g20930

A full-length Gateway clone (G83598) encoding At4g20930 was ordered from the Arabidopsis Biological Resource Center (Yamada et al., 2003). The open reading frame, which encodes a protein of 37.4 kD, was amplified by PCR, but excluding the N-terminal 84 bp, which encode a predicted mitochondrial presequence of 28 amino acids (Supplemental Fig. S3). For the overexpression of At4g20930 in *E. coli*, the Gateway pDEST17 vector was used, which allows expression of the protein in frame with an N-terminal 6× His tag. The overexpressed fusion protein was partly soluble if *E. coli* cells were cultivated at 16°C (at higher temperatures, the protein formed inclusion bodies). The protein was successfully affinity purified, as documented by SDS-PAGE and immunoblotting using an IgG directed against the His tag (Fig. 1). Furthermore, mass spectrometry (MS) analysis of the purified protein revealed that the generated transcripts are translated in the correct frame and that the protein is complete (Table I; Supplemental Fig. S4; Supplemental Table S1). The overexpressed protein is very pure (Fig. 1). MS analyses of two minor protein bands at 75 and 30 kD did not lead
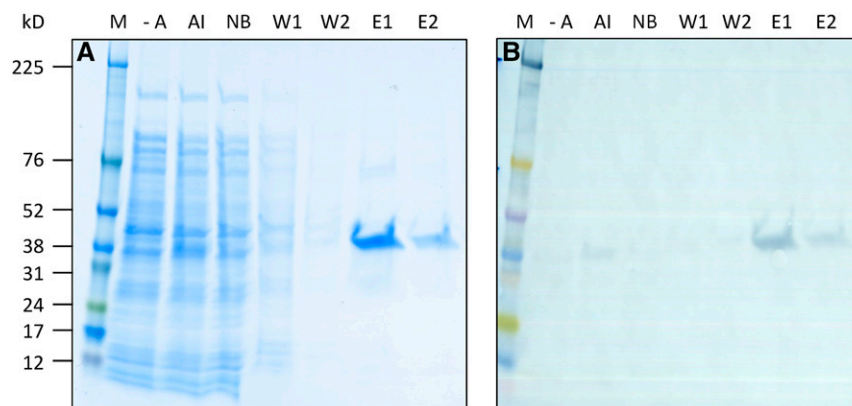
Figure 1. Expression and affinity purification of recombinant AtHDH1. A, Progression of AtHDH1 overexpression in *E. coli* and subsequent steps for AtHDH1 purification. Protein fractions were resolved by SDS-PAGE. The gel was Coomassie Blue stained. M, Marker (5 μL); –A, protein fraction of noninduced cell lysate (5 μg); AI, protein fraction after induction of the AtHDH1 gene by arabinose for 24 h at 16°C (5 μg); NB, soluble protein fraction not bound to Ni-NTA agarose beads (5 μg); W1, protein fraction of the first washing step (15 μL); W2, protein fraction of the second washing step (15 μL); E1, first protein fraction eluted from the Ni-NTA agarose beads (recombinant AtHDH1); E2, second protein fraction eluted from the Ni-NTA agarose beads (recombinant AtHDH1). B, Corresponding western blot. Recombinant AtHDH1 was detected using a horseradish peroxidase-coupled His antibody.

to the detection of any endogenic *E. coli* dehydrogenases (Supplemental Table S1).

Enzyme Properties of At4g20930

The substrate specificity of the purified protein was systematically tested by photometric activity assays using NAD$^+$ as a cosubstrate (Table II). Tested compounds were selected either because they were found to be substrates of previously characterized bacterial and/or mammalian 3-hydroxyisobutyrate dehydrogenases or because they exhibit structural similarities to 3-hydroxyisobutyrate. The substrate screening revealed highest activity of the purified enzyme for 3-hydroxyisobutyrate (4.61 μM mg^{-1} min^{-1} = 100%). To a minor extent, 3-hydroxypropionate also is converted by the enzyme (13% activity compared with 3-hydroxyisobutyrate). 3-Hydroxypropionate is an intermediate of the suggested conversion of propionyl-CoA into acetyl-CoA, which represents the final phase of the Val and Ile catabolic pathways. Furthermore, purified At4g20930 showed some low activity with methyl-3-hydroxy-2-methylpropionate as substrate (1.2%). Methyl-3-hydroxy-2-methylpropionate has an additional methyl group at the carboxyl group in

comparison with 3-hydroxyisobutyrate and was reported to be one of the major volatile components in the mammee apple (*Mammea americana*) fruit (Morales and Duque, 2002). Remarkably, the *R*-enantiomer of 3-hydroxyisobutyrate was only converted with 2% activity in comparison with the *S*-enantiomer. The *R*-enantiomer of methyl-3-hydroxy-2-methylpropionate was not converted at all by the enzyme. These results reflect a very high stereospecificity of the enzyme. Other tested compounds did not reveal any activity (Table II). For instance, glycerate, serine, as well as β-hydroxypyruvate are no substrates for the enzyme, although these compounds have similar structures to 3-hydroxyisobutyrate. We conclude that At4g20930 encodes a 3-hydroxyisobutyrate dehydrogenase. The enzyme was designated AtHDH1.
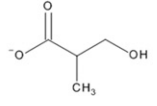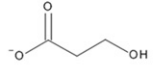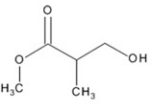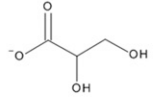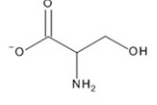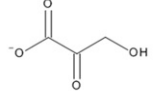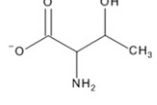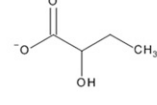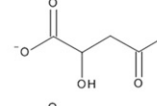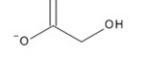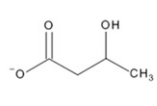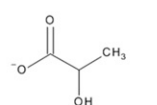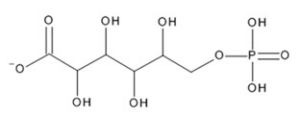
K_m and K_{cat} (turnover rate) values of AtHDH1 from Arabidopsis were determined using freshly purified protein, 3-hydroxyisobutyrate as substrate, and NAD$^+$ as cosubstrate. The calculated K_m values were 686 and 350 μM for 3-hydroxyisobutyrate and NAD$^+$, respectively (Table III). The turnover rate K_{cat} was 3.43 s^{-1} for 3-hydroxyisobutyrate and 2.652 s^{-1} for NAD$^+$. This implies a catalytic efficiency (K_{cat}/K_m) of 4.993 and 7.571 for 3-hydroxyisobutyrate and NAD$^+$, respectively. The reaction mechanism catalyzed by AtHDH1 is a

Table I. *Identification of overexpressed AtHDH1 (Fig. 1, protein band visible in lane E1) by MS*

Accession[a]	Name[b]	Mass[c]	MASCOT Score[d]	Peptides[e]	SC[f]
At4g20930	AtHDH1 (currently annotated as 6-phosphogluconate dehydrogenase family protein)	37.4	1,296	31	54.9

[a]Accession number.　　[b]Name of the identified protein.　　[c]Calculated molecular mass (kD).　　[d]Probability score for the protein identification based on the MS data and MASCOT search.　　[e]Number of unique identified peptides.　　[f]Sequence coverage (%) of the protein by identified peptides (Supplemental Fig. S4).

Table II. *Enzymatic activities of recombinant AtHDH1 using different substrates and NAD$^+$ as electron acceptor*

Substrate		Relative activity [%]
	3-Hydroxyisobutyrate	100 % S-Enantiomer 2 % R-Enantiomer
	3-Hydroxypropionate	13 %
	Methyl-3-Hydroxy-2-Methylpropionate	1,2 % S-Enantiomer 0 % R-Enantiomer
	Glycerate	0 % S-Enantiomer 0 % R-Enantiomer
	Serine	0 % S-Enantiomer 0 % R-Enantiomer
	Beta-Hydroxypyruvate	0 %
	Threonine	0 % S-Enantiomer 0 % R-Enantiomer
	2-Hydroxybutyrate	0 % S-Enantiomer 0 % R-Enantiomer
	Malate	0 % S-Enantiomer 0 % R-Enantiomer
	Glycolate	0 %
	Beta-Hydroxybutyrate	0 % S-Enantiomer 0 % R-Enantiomer
	Lactate	0 % S-Enantiomer 0 % R-Enantiomer
	6-Phosphogluconate	0 %

Activity was measured using the standard conditions described in "Materials and Methods." The activity of the substrate S-3-hydroxyisobutyrate was defined to be 100%.

sequential bibi mechanism common for most dehydrogenases (Supplemental Fig. S5). Both substrates (3-hydroxyisobutyrate and NAD$^+$) have to bind before either product is released. The pH optimum of AtHDH1 is 8.5 (Fig. 2A), which is close to the estimated pH value of 8.1 for the mitochondrial matrix in Arabidopsis as determined by a mitochondria-specific fluorescence pH sensor (Shen et al., 2013). Enzyme activity measurements at varying temperatures revealed a wide temperature range. The optimum activity is at about 40°C (Fig. 2B). Above 50°C, the enzyme activity declines.

Arabidopsis AtHDH1 is highly specific for NAD$^+$ as a cofactor. NADP$^+$ is not a suitable cofactor for AtHDH1. Also, FAD, oxidized cytochrome *c*, as well as the artificial electron acceptors phenazine methosulfate (PMS) and dichlorophenol indophenol cannot be reduced by AtHDH1 (data not shown).

In parallel, another Arabidopsis protein, At4g29120, which slightly resembles AtHDH1, was overexpressed in *E. coli* and affinity purified (Supplemental Fig. S6). This protein did not exhibit any 3-hydroxyisobutyrate dehydrogenase activity. We conclude that HDH is encoded by single-copy gene. Furthermore, lack of activity in overexpressed At4g29120 fractions further excludes that the *E. coli* background of our protein expression system interfered with our biochemical characterization of overexpressed AtHDH1.

The Native State of AtHDH1

The native state of AtHDH1 from Arabidopsis was tested by analyzing the purified recombinant protein using blue native PAGE in combination with a 3-hydroxyisobutyrate dehydrogenase in-gel activity assay (Fig. 3). Due to a high Coomassie Blue background in the low-molecular-mass region of the gel, the activity of the monomer could not be seen. Activity signals were visible at about 150, 187, 200, and 224 kD. Since the overexpressed protein is of high purity, we conclude that AtHDH1 can form homooligomeric protein complexes. Dimeric and tetrameric forms of HDH1 were described previously for several organisms (Rougraff et al., 1988; Lokanath et al., 2005). The 150-kD band nicely corresponds to the expected mass of a tetramer. The 187- and 224-kD bands could represent pentamers or hexamers. The identity of the 200-kD band is not clear.

Table III. *Kinetic parameters of recombinant 3-hydroxyisobutyrate dehydrogenase from Arabidopsis using 3-hydroxyisobutyrate and NAD$^+$ as substrates*

Parameter	3-Hydroxyisobutyrate	NAD$^+$
K_m (mM)	0.687 ± 0.198	0.350 ± 0.152
K_{cat} (s^{-1})	3.430 ± 0.279	2.652 ± 0.264
K_{cat}/K_m (s^{-1} mM^{-1})	4.993	7.571

Kinetic data were fitted by using nonlinear regression analysis. The values represent means ± SE of three independent enzyme preparations.
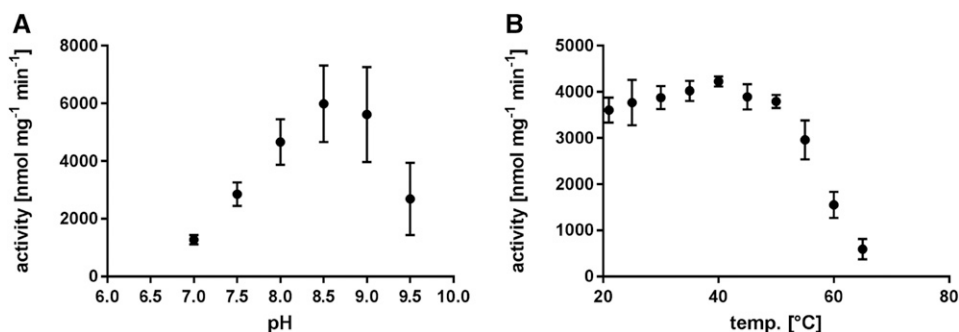
Figure 2. pH and temperature optima of overexpressed AtHDH1 from Arabidopsis. A, pH optima. The activity of AtHDH1 was measured in a buffer containing 250 mm Tris-HCl, pH 7 to 9.5, 5 mm NAD$^+$, and 5 mm 3-hydroxyisobutyrate. B, Temperature optima of AtHDH1. The activity of AtHDH1 was measured at 20°C to 65°C in a buffer containing 250 mm K$_2$HPO$_4$ × KH$_2$PO$_4$, pH 7.5, 5 mm NAD$^+$, and 10 mm 3-hydroxyisobutyrate.

Characterization of Arabidopsis AtHDH1 Knockdown Lines

Arabidopsis lines carrying T-DNA insertions in the gene encoding At4g20930 were ordered to investigate the physiological role of AtHDH1. Overall, six mutant lines are available, termed ΔHDH1-1 to ΔHDH1-6 (Fig. 4). The exact positions of the insertions were determined by DNA sequencing for lines ΔHDH1-2, ΔHDH1-4, and ΔHDH1-6. Line ΔHDH1-4 carries an insertion 471 bp upstream of the transcription initiation site, which is usually considered to be outside the promotor region in

Figure 3. Native molecular mass of 3-hydroxyisobutyrate dehydrogenase. A protein fraction containing recombinant AtHDH1 was separated by blue native PAGE. The gel was stained for AtHDH1 activity. Proteins of a molecular mass standard (M) were separated in parallel (the masses of the standard proteins are given to the left in kD). Apparent native molecular masses of HDH1 are indicated to the right of the activity stain.

Arabidopsis (Kleinboelting et al., 2012; Shahmuradov et al., 2017). Insertions in ΔHDH1-1 and ΔHDH1-5 are even farther upstream (Fig. 4). All three lines were discarded for further analyses because the insertions probably do not affect the expression of the AtHDH1 gene. The T-DNA insertion of another line (ΔHDH1-3) could not be confirmed by the GABI-Kat consortium. For these reasons, all further experiments were carried out using lines ΔHDH1-2 (GK-911G06) and ΔHDH1-6 (GK-710H08). Line ΔHDH1-6 carries the insertion within the 5′ untranslated region (9 bp upstream of the transcript initiation site) and line ΔHDH1-2 within intron 6 (Fig. 4). Both lines are homozygous with respect to the T-DNA insertion, as confirmed by PCR (Supplemental Fig. S7). HDH1 expression is reduced by around 50% in the two mutant lines (Fig. 5). We conclude that both lines represent knockdown lines. HDH1 knockout lines possibly are not viable because disruption of the hdh1 gene causes an embryo-lethal defect.
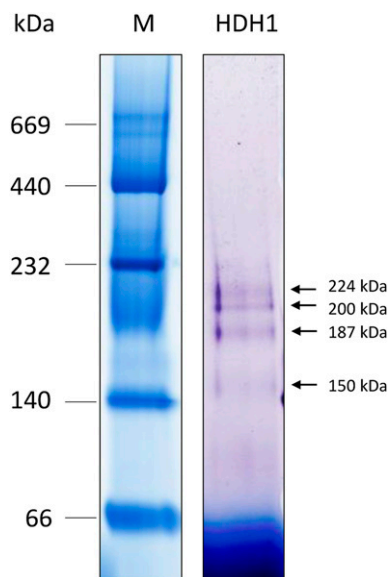
ΔHDH1 Knockdown Lines Are Deficient in Val and Ile But Not in Leu Breakdown

Plants of the Arabidopsis lines ΔHDH1-2 and ΔHDH1-6 had no visible phenotypes under the conditions tested. Plants were cultivated in long-day conditions and short-day conditions. Even upon extended darkness for 7 d, no phenotypic differences were visible between wild-type plants and the knockdown mutants (Supplemental Fig. S8). The progress of chlorosis was similar in all lines. We conclude that reduction in AtHDH1 expression is not strong enough to cause a visible phenotype. Therefore, root toxicity assays were carried out to use a more sensitive experimental system for monitoring phenotypic effects of the T-DNA insertion line.

Wild-type plants and plants of the AtHDH1 knockdown lines ΔHDH1-2 and ΔHDH1-6 were cultivated under sterile conditions on agar plates for 4 d. Subsequently, plant cultivation was continued on agar plates, which were supplemented with either 250 and 500 μM Val or with 50 and 100 μM Leu/Ile. After 10 d of further
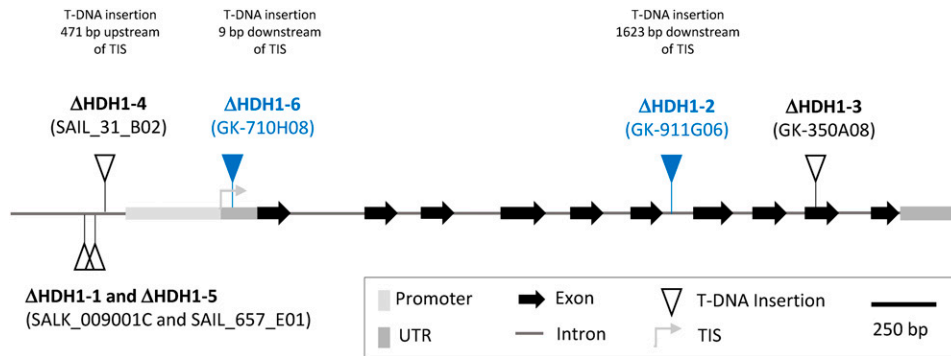
Figure 4. Model of the gene encoding 3-hydroxyisobutyrate dehydrogenase from Arabidopsis. The promoter region is shown in light gray. The 5′ and 3′ untranslated regions (UTR) are shown in dark gray. Exons are indicated by black arrows and introns by the gray line. Available T-DNA insertion lines are indicated by triangles (ΔHDH1-1–ΔHDH1-6 are SALK, SAIL, or GABI-Kat lines). The exact positions of the T-DNA insertions were determined by sequence analyses for lines ΔHDH1-2, ΔHDH1-4, and ΔHDH1-6. All experiments of our study were carried out using lines ΔHDH1-2 and ΔHDH1-6 (insertions indicated by blue triangles). TIS, Transcription initiation site.

cultivation, roots were scanned and root length was calculated using the AxioVision Microscope Software (Carl Zeiss). The cultivation of plants in the presence of excess Val and Ile clearly increased root growth inhibition in the mutant with respect to wild-type plants (Fig. 6). In contrast, root growth in the presence of Leu did not cause a decrease in root growth in the mutant line compared with the wild-type line. The observed root inhibition effects in the AtHDH1 knockdown line were of moderate intensity, which probably is caused by the remaining AtHDH1 expression (Fig. 5). We conclude that AtHDH1 is involved in the breakdown of Val and Ile but not of Leu.
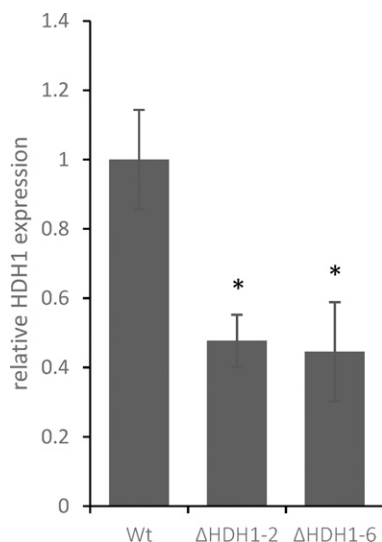

Figure 5. Relative AtHDH1 expression in ΔHDH1-2 and ΔHDH1-6 knockdown lines. Relative expression was determined by reverse transcription-quantitative PCR (n = 3). Actin was used for normalization. Wt, Wild type. Asterisks show significant differences compared with the wild type according to Student's t test ($P < 0.05$).

DISCUSSION

Plants can generate ATP from ADP and inorganic phosphate in various ways. In the light, ATP mainly comes from photophosphorylation taking place in the chloroplasts. At the same time, as in heterotrophic eukaryotes, ATP is generated in the mitochondria by oxidative phosphorylation. The latter process is the main ATP-generating process in plants in the absence of light (e.g. at night) or in nongreen tissue (e.g. roots). For oxidative phosphorylation, plants have to fuel the electron transport chain with electrons, which mainly come from the oxidation of carbohydrates via glycolysis and the citric acid cycle. However, under special abiotic as well as biotic stress conditions, carbohydrates can become limiting and oxidation of other compounds becomes important for providing electrons to the mitochondrial electron transport chain. The oxidation of BCAAs was found to be very important for the respiration of plant cells under carbon starvation conditions (Ishizaki et al., 2005, 2006; Araújo et al., 2010). In BCAA catabolism, BCKDH generates NADH. We here report the identification of a second NADH-generating enzyme of the BCAA degradation pathway, AtHDH1. The suggested role of the enzyme in BCAA catabolism is summarized in Figure 7. Besides BCKDH and AtHDH1, the existence of a third enzyme, methylmalonate-semialdehyde dehydrogenase, is predicted to produce NADH. The formed NADH can transfer electrons to the NADH dehydrogenase complex (complex I) or to one of the alternative NAD(P)H dehydrogenases forming part of the respiratory chain in plants (Rasmusson et al., 2004). Furthermore, IVDH, another enzyme of the BCAA catabolic pathway, contributes electrons to the respiratory chain. However, this enzyme directly transfers electrons via the ETF/ETFQO system to ubiquinone. Finally, BCAA catabolism leads to the formation of acetyl-CoA, which is a substrate of the citric acid cycle. Complete oxidation of the acetyl group generates another three NADHs and one $FADH_2$.
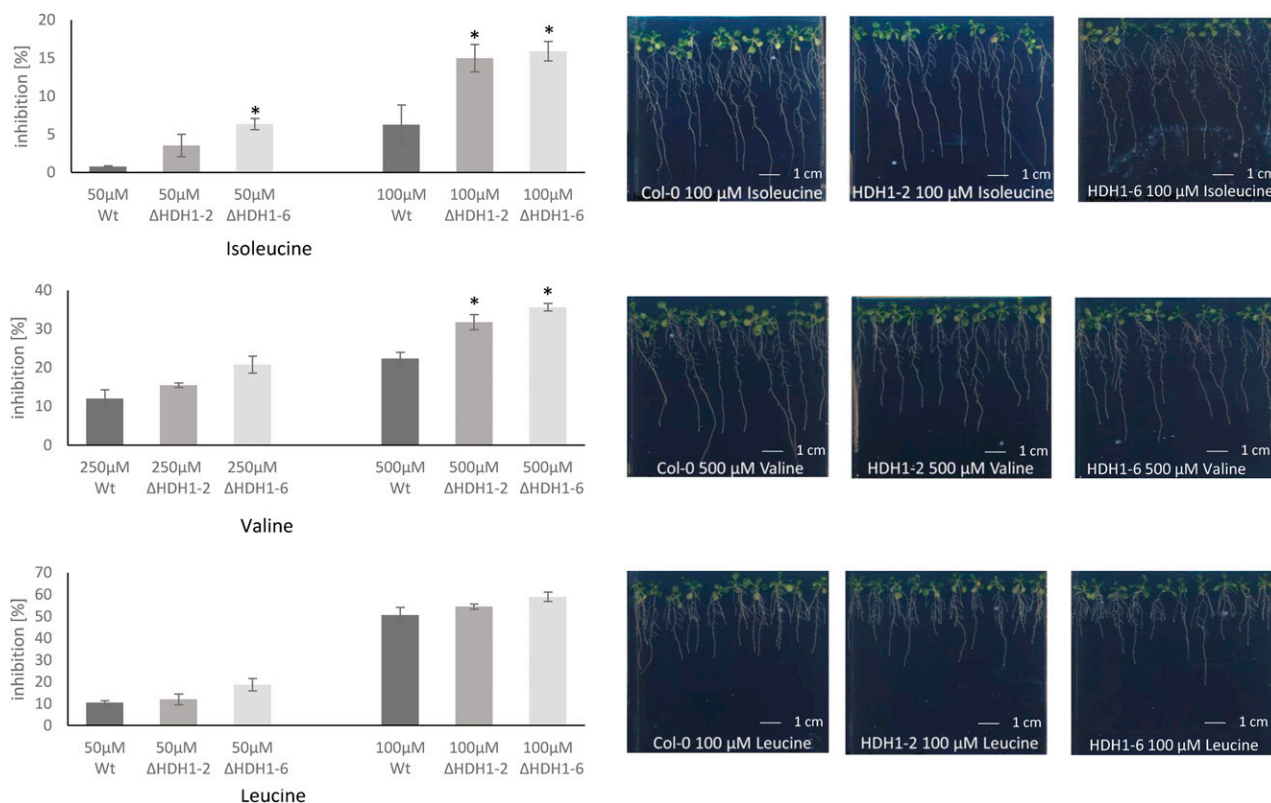
Figure 6. AtHDH1-2 shows impaired root growth in the presence of Val and Ile. Arabidopsis lines (wild type [Wt], AtHDH1-2, and AtHDH1-6) were grown on one-half-strength Murashige and Skoog plates for 4 d before being transferred to one-half-strength Murashige and Skoog plates supplemented with Val (250 and 500 μM), Ile (50 and 100 μM), or Leu (50 and 100 μM). Inhibition percentage is shown in comparison with plants of each line grown on control plates. The results are derived from three different experiments with 20 plants (two plates) per treatment. Shown are mean values ± SE. Asterisks show significant differences compared with the wild type according to Student's t test ($P < 0.05$). Images to the right of the graphs show the effects of the treatments on root growth.

In summary, BCAA degradation can greatly contribute to oxidative phosphorylation at carbohydrate limitation. Nevertheless, Leu, Ile, and Val catabolism has not been much studied in plants so far. We here report the characterization of one of the so-far unknown enzymes of the BCAA degradation pathway in plants, AtHDH1 (At4g20930). A second putative HDH gene was recently predicted, At4g29120 (Hildebrandt et al., 2015). The amino acid sequence identity between At4g29120 and At4g20930 is 32%. We also recombinantly expressed At4g29120 in *E. coli* (Supplemental Fig. S6). However, the purified protein did not exhibit 3-hydroxyisobutyrate dehydrogenase activity (Supplemental Fig. S6). We cannot exclude that the overexpressed protein was inactive due to misfolding or aggregation. However, our results here rather indicate that HDH is encoded by a single-copy locus in Arabidopsis. In contrast, HDH isoforms have been described for mammalian mitochondria (Loupatty et al., 2006).

AtHDH1 was shown to be a highly active 3-hydroxyisobutyrate dehydrogenase. In addition, 3-hydroxypropionate and methyl-3-hydroxy-2-methylpropionate also are substrates for AtHDH1.

No activity could be measured using glycerate or serine as substrate. This is in contrast to HDH from mammalian mitochondria. The enzyme from rat is active with a series of 3-hydroxyacid substrates, including *S*- and *R*-hydroxyisobutyrate, L-glycerate, and L-Ser (Hawes et al., 1996). In our study, AtHDH1 shows high specificity for *S*-enantiomers, as reported for the majority of HDHs from microorganisms and mammals (Hasegawa, 1981). AgNO$_3$ is a strong inhibitor of AtHDH1 activity (data not shown). This points to the presence of sulfhydryl groups close to the 3-hydroxyisobutyrate- or NAD$^+$-binding sites. The optimal pH for AtHDH1 is around 8.5. Also, HDH from different mammals show a basic pH optimum (Robinson and Coon, 1957; Tasi et al., 2013). The temperature optimum of AtHDH1 is around 40°C, and the enzyme shows a wide activity range between 20°C and 50°C, which reflects the conditions of natural Arabidopsis habitats. The AtHDH1 knockdown plants used in our study had no visible phenotype under the conditions tested, even under extended darkness, which most likely is due to the remaining AtHDH1 expression. However, more sensitive root toxicity assays revealed a role of AtHDH1 in BCAA catabolism.

Figure 7. BCAA catabolism in plants (modified from Hildebrandt et al., 2015). Enzymes are underlaid by gray circles (BCAT, branched-chain amino acid transaminase; MCCase, methylcrotonyl-CoA carboxylase; ECH, enoyl-CoA hydratase; HL, hydroxmethylglutaryl-CoA lyase; HCDH, 3-hydroxyacyl-CoA dehydrogenase; KCT, 3-ketoacyl-CoA thiolase; HADH, hydroxyacyl-CoA hydrolase; MMSDH, methylmalonate-semialdehyde dehydrogenase; ACOX, acyl-CoA oxidase; ACAT, acetyl-CoA acetyltransferase). Some key substrates, cosubstrates, and products are underlaid in blue (Leu, Ile, and Val). The two enzymatic steps catalyzed by HDH are underlaid in green.
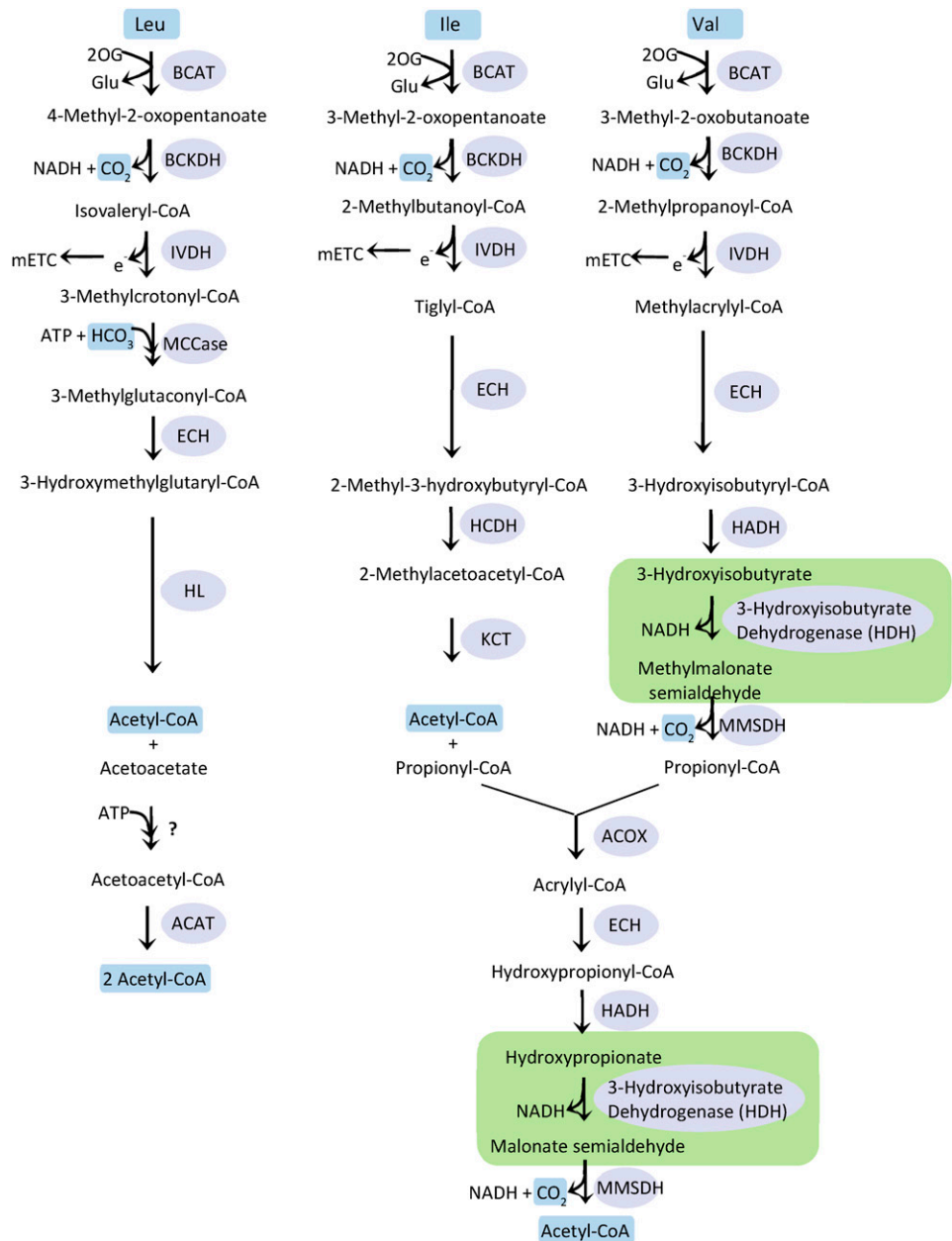
The 3-hydroxyisobutyrate dehydrogenase from *Thermus thermophilus* has been crystallized and shown to be a homotetrameric enzyme (Lokanath et al., 2005). Similarly, AtHDH1 might form homooligomeric complexes. Activity signals of the recombinantly expressed protein could be detected in the molecular mass range from 150 to 225 kD upon blue native PAGE (Fig. 3). This might indicate that AtHDH1 forms tetrahomomeric to hexahomomeric complexes. However, these results have to be taken with caution, because artificial aggregations of AtHDH1 overexpressed in *E. coli* cannot be excluded.

According to currently available information, the first four enzymatic steps of Val, Ile, and Leu degradation are carried out by the same set of enzymes in plants (Hildebrandt et al., 2015), with an enoyl-CoA hydratase representing the last enzyme acting in all three degradation pathways (Fig. 7). In Val degradation, hydroxyisobutyrate is produced from hydroxyisobutyryl-CoA. This step distinguishes the Val catabolic pathway from Leu and Ile degradation. In Leu as well as Ile degradation, no CoA liberation takes place at this step. AtHDH1 converts 3-hydroxyisobutyrate to methylmalonate semialdehyde. Root toxicity experiments with mutant lines show the involvement of AtHDH1 in Val degradation. Cultivation of AtHDH1 knockdown mutants in the presence of excess of Val inhibits root growth stronger than in wild-type plants (Fig. 6). In the next step, CoA is again attached. This step is carried out by the methylmalonate

semialdehyde dehydrogenase. The mammalian enzyme is unique among known aldehyde dehydrogenases because it is CoA dependent (Kedishvili et al., 1992). It is assumed that propionyl-CoA is produced in Val as well as in Ile degradation (Fig. 7). Finally, it has been suggested that at least five enzymes are required to convert propionyl-CoA into acetyl-CoA (Hildebrandt et al., 2015). We present evidence that AtHDH1 is among these five enzymes. AtHDH1 is capable of converting 3-hydroxypropionate into malonate semialdehyde (Table II). Indeed, root toxicity experiments using the AtHDH1 knockdown mutants revealed that growth inhibition increased not only upon cultivation of plants in the presence of Val but also in the presence of Ile (Fig. 6). This double role of HDH also has be reported for 3-hydroxyisobutyrate dehydrogenase from microorganisms (Yao et al., 2010). In contrast, according to available experimental data, HDH seems to be involved only in Val degradation in animals. Further investigation of BCCA catabolism in plants will be required to better understand the plant-specific features and the physiological function of BCAA catabolism in the context of photoautotrophic life.

MATERIALS AND METHODS

Expression and Purification of Recombinant AtHDH1

The nucleotide sequence encoding Arabidopsis (*Arabidopsis thaliana*) AtHDH1 was amplified from a Gateway clone (G83598; Arabidopsis Biological Resource Center). The first 84 bp of the open reading frame were excluded because it encodes the N-terminal presequence as predicted by MitoFates Fukasawa et al. 2015 (http://mitf.cbrc.jp/MitoFates/cgi-bin/top.cgi; Supplemental Fig. S3). The forward PCR primer contained the sequence CACC at the 5′ end to enable directional TOPO cloning. The following primers were used: AtHDH1_FWD_w/o_Mito (5′-CACCTCTTCGTCTCAAAATTCAA-3′) and AtHDH1_RV_w/o_Mito (5′-TCAGACCTCATCTTTCCCATTG-3′). PCR was carried out using Phusion High-Fidelity DNA Polymerase (Thermo Fisher Scientific) to create blunt-end PCR products. The following conditions were applied: initial denaturation at 95°C for 5 min; followed by 37 cycles of denaturation at 95°C for 30 s, annealing at 67.5°C for 30 s, and elongation at 72°C for 90 s; and a final elongation step at 72°C for 5 min. The obtained DNA fragment was cloned into the pENTR/D-TOPO vector using the pENTR Directional TOPOCloning Kit (Thermo Fisher Scientific). The resulting plasmid was called pENTR-D-TOPO-AtHDH1-w/o-28-AA. After transformation of the plasmid in One Shot Chemically Competent *Escherichia coli* cells (contained in the pENTR Directional TOPOCloning Kit) and overnight culturing on Luria-Bertani (LB) agar plates supplemented with 50 μg mL^{-1} kanamycin, single colonies were picked and propagated overnight at 37°C in LB medium at 170 rpm. Afterward, the plasmid DNA was isolated using the GeneJET Plasmid Miniprep Kit (Thermo Fisher Scientific). The plasmid was sequenced by SEQLAB (SEQLAB Sequence Laboratories). Afterward, the LR recombination reaction using the Gateway LR Clonase II Enzyme Mix (Thermo Fisher Scientific) was performed to clone AtHDH1 into the Gateway pDEST17 vector so that AtHDH1 can be expressed in frame with an N-terminal 6× His tag. The resulting expression plasmid was designated pDest17-AtHDH1-w/o-28-AA. Next, the plasmid was transformed into NEB 5-alpha (New England Biolabs) competent cells and grown overnight on LB agar plates supplemented with 50 μg mL^{-1} carbenicillin. Single colonies were picked and grown in LB medium at 37°C and shaking at 170 rpm in the presence of 50 μg mL^{-1} carbenicillin. The correct sequence of plasmids was checked by sequencing (SEQLAB Sequence Laboratories).

For AtHDH1 expression, pDest17-AtHDH1-w/o-28-AA was transformed in BL21-AI One Shot Chemically Competent *E. coli* cells (Thermo Fisher Scientific). In these cells, the T7-RNA polymerase gene is under the control of the *araBAD* promoter. Transformed cells were grown in LB medium supplemented with 50 μg mL^{-1} carbenicillin at 37°C until the OD$_{600}$ reached 0.6 to 1. AtHDH1 expression was induced using 0.05% (w/v) L-arabinose. Starting from this time

point, bacteria were transferred to 16°C for 24 h in order to decrease the risk of inclusion body formation. Bacteria were lysed according to the manufacturer's instructions using BugBuster Master Mix (Merck Millipore). The soluble fraction was used for affinity purification using immobilized metal ion chromatography on Ni-NTA agarose (Qiagen). NaCl (1 M) and 20 mM imidazol as final concentrations were added to the supernatant to prevent the unspecific binding of non-His-tagged proteins. The beads were equilibrated and washed with 33 mM NaH$_2$PO$_4$, 2 M NaCl, and 53 mM imidazol. The protein was eluted using 50 mM NaH$_2$PO$_4$, 300 mM NaCl, and 400 mM imidazol. Desalting was achieved by using Microcon-30kDa centrifugal filters (Merck Millipore). After 10 min of centrifugation at 14,000g, 200 μL of 20 mM K$_2$HPO$_4$, pH 8, was added and again centrifuged for 10 min at 14,000g. The freshly desalted protein was immediately used to determine K_m and K_{cat} or 20% (v/v) glycerol was added for protein storage at −20°C for a short term.

Enzyme Activity Assays and Substrate Screening

The standard 3-hydroxyisobutyrate dehydrogenase assay took place in a buffer composed of 250 mM Tris-HCl, pH 8.5, 5 mM NAD$^+$, 200 ng of AtHDH1 (from at least a minimum of three different enzyme batches from elution fraction 2), and 5 mM 3-hydroxyisobutyrate. Elution fraction 2 was used in order to have a very pure fraction for experiments. Assays were carried out in a total volume of 300 μL in the wells of a 96-well plate. The production of NADH ($\varepsilon_{340} = 6.22$ mM^{-1} cm^{-1}) was measured at 340 nm using an Epoch Microplate Spectrophotometer (Biotek). Enzyme assays were carried out at 25°C. Kinetic values were corrected by values obtained in parallel control experiments (assays without substrate or added protein). Protein quantification was carried out using the Pierce Coomassie (Bradford) Protein Assay (Thermo Fisher Scientific).

The K_m and V_{max} values were determined at pH 8.5 by varying the concentration of the substrate while keeping the concentrations of the other components constant. At least three different enzyme batches were used, and kinetic constants were calculated using nonlinear regression (Graph Pad Prism 7; GraphPad Software).

Substrate screening was carried out in a buffer containing 250 mM Tris-HCl, pH 8.5, 5 mM NAD$^+$, different amounts of recombinantly expressed AtHDH1, and 10 mM substrate. The substrates tested were 3-hydroxyisobutyrate, 3-hydroxypropionate, methyl-3-hydroxy-2-methylpropionate, glycerate, serine, β-hydroxypyruvate, threonine, 2-hydroxybutyrate, malate, glycolate, β-hydroxybutyrate, lactate, and 6-phosphogluconate.

To determine the pH optimum of AtHDH1, a buffer mixture was used containing 250 mM Tris-HCl, pH 7 to 9.5, 5 mM NAD$^+$, and different amounts of recombinantly expressed AtHDH1 The reaction was started with 5 mM 3-hydroxyisobutyrate and took place at a final volume of 300 μL.

The temperature optimum of AtHDH1 was tested using a buffer including 250 mM K$_2$HPO$_4$ × KH$_2$PO$_4$, pH 7.5 (since the pH of a Tris-HCl buffer changes with different temperatures, we decided to use a potassium phosphate buffer).

Cofactors were analyzed using the standard assay conditions. However, NAD$^+$ was replaced by NADP$^+$ ($\varepsilon_{340} = 6.22$ mM^{-1} cm^{-1}), cytochrome c ($\varepsilon_{550} = 19$ mM^{-1} cm^{-1}) or FAD, PMS, and dichlorophenol indophenol ($\varepsilon_{600} = 19.1$ mM^{-1} cm^{-1}).

SDS-PAGE and Western Blotting

Protein concentration was determined using the Pierce Coomassie (Bradford) Protein Assay (Thermo Fisher Scientific). SDS-PAGE was performed using precast gels from Bio-Rad. Gel runs were performed according to the manufacturer's instructions. After completion of the gel run, the gel was either stained using the Coomassie Blue colloidal procedure (Neuhoff et al., 1988) or electroblotted onto a nitrocellulose membrane for immunoblotting. Western blots were incubated with a horseradish peroxidase-conjugated 6× His, His-Tag Mouse Monoclonal Antibody (Proteintech Europe) and developed using nickel chloride combined with 3,3′-Diaminobenzidine (DAB) according to Coventry et al. (1995). The Amersham ECL Rainbow Marker-High Range was used (GE Healthcare).

Protein Identification by MS

For identification, protein bands were cut out from polyacrylamide gels, and included proteins were fragmented into peptides by trypsin treatment as described previously (Klodmann et al., 2011). Peptide mixtures were purified, and peptides were separated by liquid chromatography and analyzed by tandem MS using a micrOTOF Q-II mass spectrometer (Bruker) as outlined before (Klodmann et al., 2011).

Blue Native PAGE and In-Gel Activity Staining

Blue native PAGE was performed employing a precasted 4–16% Bis-Tris Native Gel (Thermo Fisher Scientific). The blue native cathode buffer (50 mM Tricine, 15 mM BisTris, and 0.02% [w/v] Coomassie Blue G250, pH 7) and the blue native anode buffer (50 mM BisTris, pH 7) were used. The Coomassie Blue-containing cathode buffer was replaced after half of the run by a cathode buffer without Coomassie Blue in order to strongly reduce excess Coomassie Blue. The gel run was carried out according to the manufacturer's instructions at 4°C. After the gel run was completed, in-gel activity assays were carried out by incubating gels in the dark at room temperature with 20 mL of staining solution containing 250 mM Tris-HCl, pH 8.5, 0.4 mg mL^{-1} nitroblue tetrazolium, 0.2 mM PMS, 2 mM NAD$^+$, and 5 mM 3-hydroxyisobutyrate. As a native marker, the Amersham High M_r Calibration Kit for native electrophoresis was used (GE Healthcare).

Mutant Screening

Seeds of T-DNA insertion lines ΔHDH1-1 (SALK_009001C), ΔHDH1-2 (GK-911G06), ΔHDH1-4 (SAIL_31_B02), and ΔHDH1-5 (SAIL_657_E01) were obtained from the Nottingham Arabidopsis Stock Centre (http://arabidopsis.info/). Lines ΔHDH1-6 (GK-710H08) and ΔHDH1-3 (GK-350A08) were ordered directly from GABI-Kat (https://www.gabi-kat.de/). Genomic DNA was isolated according to Edwards et al. (1991). Plants homozygous with respect to the T-DNA insertion were isolated by multiplex PCR using the following primers: ΔHDH1-2_Fw, 5'-TGGAGAAAATGATATAAGACCTGC-3'; ΔHDH1-2_Rv, 5'-TGTCTGAAAACACAAGAGAAGTC-3'; and T-DNA Primer, GABI_Kat_o8474, 5'-ATAATAACGCTGCGGACAT-3'. For ΔHDH1-6, the following primers were used: ΔHDH1-6_Fw, 5'-AATTATTTTCATGGGTTCACGAG-3'; ΔHDH1-6_Rv, 5'-CATTTTCATAACATCACGGTTTCT-3'; and T-DNA Primer, GABI_Kat_o8474, 5'-ATAATAACGCTGCGGACAT-3'. Annealing temperatures were calculated using the Tm Calculator (www.thermoscientific.com/pcrwebtools; Thermo Fisher Scientific). In order to determine the exact T-DNA insertion site, PCR products were sequenced by SEQLAB (SEQLAB Sequence Laboratories).

Gene Expression Analyses

To determine gene expression in lines ΔHDH1-2 and ΔHDH1-6, quantitative PCR analysis was carried out according to Heimann et al. (2013). First, total RNA was isolated from 100 mg of leaves using the GeneJET Plant RNA Purification Kit (Thermo Fisher Scientific). Subsequently, RNA was converted into first-strand cDNA. cDNA synthesis was performed with approximately 1 μg of total RNA and 50 pmol of random nonamer primer. Reactions were incubated for 5 min at 70°C and cooled down on ice before adding 200 units of Moloney murine leukemia virus reverse transcriptase (Promega) and 1 mM deoxyribonucleotide triphosphates in reaction buffer, as specified by the manufacturer. Quantitative PCR was performed on an ABI PRISM 7300 sequence detection system (Thermo Fisher Scientific) using SYBR Green fluorescence (Platinum SYBR Green QPCR Mix; Thermo Fisher Scientific). The following primers were used: ΔHDH1_qPCR_FW_2 (5'-CTAGTGGCCGTTGTTGGAGCAGTGA-3') and ΔHDH1_qPCR_RV_2 (5'-TCAGCTGAGGCTGCTGCGAGGT-3'). Amplification conditions were 2 min of initial denaturation at 95°C, followed by 40 cycles of 15 s at 95°C and 1 min at 60°C. Afterward, a melting curve was recorded. General reaction conditions were 3 mM MgCl$_2$ and 200 nM of each oligonucleotide. The sizes of the amplified molecules were confirmed by gel electrophoresis. At least three biological replicates were carried out for each measurement.

Cultivation of Plants on Agar Plates and Root Toxicity Assays

Seeds of ΔHDH1-2, ΔHDH1-6, and Columbia-0 were surface sterilized and sown on one-half-strength Murashige and Skoog agar plates. After 2 d at 4°C, plates were transferred to a climate chamber (16/8 h of light/dark) for continuation of plant cultivation at 22°C and 85 μmol s^{-1} m^{-2} light. After 4 d in the climate chamber, 10 seedlings with approximately the same size and the same root length were transferred to one-half-strength Murashige and Skoog agar plates, which were supplemented with 250 and 500 μM Val or 50 and 100 μM Leu/Ile. Control plates did not contain any amino acids. After 10 d, plates were scanned, and the root lengths were determined with the AxioVision Microscope Software (Carl Zeiss). The results are derived from three different biological

experiments each with 20 plants (two plates) per treatment (in total, 60 plantlets were measured per treatment and concentration).

Supplemental Data

The following supplemental materials are available.

Supplemental Figure S1. Alignment of At4g20930 and human 3-hydroxyisobutyrate dehydrogenase using ClustalΩ.

Supplemental Figure S2. HDH1 has been identified in a mitochondrial fraction of Arabidopsis.

Supplemental Figure S3. HDH1 has a predicted presequence comprising 28 amino acids.

Supplemental Figure S4. Sequence coverage of HDH1 from Arabidopsis by peptides identified by MS.

Supplemental Figure S5. The reaction mechanism catalyzed by AtHDH1 is a sequential bibi mechanism.

Supplemental Figure S6. Affinity purification of recombinant At4g29120 and activity with 3-hydroxyisobutyrate as substrate

Supplemental Figure S7. Identification of Arabidopsis lines homozygous for T-DNA insertions in At4g20930.

Supplemental Figure S8. HDH1 knockdown mutants under extended darkness conditions.

Supplemental Table S1. Proteins identified in the 75-, 37-, and 30-kD bands of the SDS gel shown in Figure 1 by MS using the SwissProt database.

LITERATURE CITED

Alban C, Baldet P, Axiotis S, Douce R (1993) Purification and characterization of 3-methylcrotonyl-coenzyme A carboxylase from higher plant mitochondria. Plant Physiol **102:** 957–965

Anderson MD, Che P, Song J, Nikolau BJ, Wurtele ES (1998) 3-Methylcrotonyl-coenzyme A carboxylase is a component of the mitochondrial leucine catabolic pathway in plants. Plant Physiol **118:** 1127–1138

Angelovici R, Lipka AE, Deason N, Gonzalez-Jorge S, Lin H, Cepela J, Buell R, Gore MA, Dellapenna D (2013) Genome-wide analysis of branched-chain amino acid levels in Arabidopsis seeds. Plant Cell **25:** 4827–4843

Araújo WL, Ishizaki K, Nunes-Nesi A, Larson TR, Tohge T, Krahnert I, Witt S, Obata T, Schauer N, Graham IA, et al (2010) Identification of the 2-hydroxyglutarate and isovaleryl-CoA dehydrogenases as alternative electron donors linking lysine catabolism to the electron transport chain of Arabidopsis mitochondria. Plant Cell **22:** 1549–1563

Araújo WL, Tohge T, Ishizaki K, Leaver CJ, Fernie AR (2011) Protein degradation: an alternative respiratory substrate for stressed plants. Trends Plant Sci **16:** 489–498

Binder S (2010) Branched-chain amino acid metabolism in Arabidopsis thaliana. The Arabidopsis Book **8:** e0137, doi/10.1199/tab.0137

Chowdhury EK, Akaishi Y, Nagata S, Misono H (2003) Cloning and overexpression of the 3-hydroxyisobutyrate dehydrogenase gene from pseudomonas putida E23. Biosci Biotechnol Biochem **67:** 438–441

Coventry BJ, Bradley J, Skinner JM (1995) Differences between standard and high-sensitivity immunohistology in tissue sections: comparison of immunoperoxidase staining methods using computerized video image analysis techniques. Pathology **27:** 221–223

Däschner K, Couée I, Binder S (2001) The mitochondrial isovaleryl-coenzyme A dehydrogenase of Arabidopsis oxidizes intermediates of leucine and valine catabolism. Plant Physiol 126: 601–612

Edwards K, Johnstone C, Thompson C (1991) A simple and rapid method for the preparation of plant genomic DNA for PCR analysis. Nucleic Acids Res 19: 1349

Fukasawa Y, Tsuji J, Fu SC, Tomii K, Horton P, Imai K (2015) MitoFates: improved prediction of mitochondrial targeting sequences and their cleavage sites. Mol Cell Proteomics 14: 1113–1126

Harper AE, Miller RH, Block KP (1984) Branched-chain amino acid metabolism. Annu Rev Nutr 4: 409–454

Hasegawa J (1981) Distribution in organisms and stereospecificity of β-hydroxyisobutyrate dehydrogenase. Agric Biol Chem 45: 2899–2901

Hawes JW, Crabb DW, Chan RM, Rougraff PM, Harris RA (1995) Chemical modification and site-directed mutagenesis studies of rat 3-hydroxyisobutyrate dehydrogenase. Biochemistry 34: 4231–4237

Hawes JW, Harper ET, Crabb DW, Harris RA (1996) Structural and mechanistic similarities of 6-phosphogluconate and 3-hydroxyisobutyrate dehydrogenases reveal a new enzyme family, the 3-hydroxyacid dehydrogenases. FEBS Lett 389: 263–267

Heimann L, Horst I, Perduns R, Dreesen B, Offermann S, Peterhansel C (2013) A common histone modification code on C4 genes in maize and its conservation in Sorghum and Setaria italica. Plant Physiol 162: 456–469

Hildebrandt TM, Nunes Nesi A, Araújo WL, Braun HP (2015) Amino acid catabolism in plants. Mol Plant 8: 1563–1579

Ishizaki K, Larson TR, Schauer N, Fernie AR, Graham IA, Leaver CJ (2005) The critical role of Arabidopsis electron-transfer flavoprotein: ubiquinone oxidoreductase during dark-induced starvation. Plant Cell 17: 2587–2600

Ishizaki K, Schauer N, Larson TR, Graham IA, Fernie AR, Leaver CJ (2006) The mitochondrial electron transfer flavoprotein complex is essential for survival of Arabidopsis in extended darkness. Plant J 47: 751–760

Joshi V, Joung JG, Fei Z, Jander G (2010) Interdependence of threonine, methionine and isoleucine metabolism in plants: accumulation and transcriptional regulation under abiotic stress. Amino Acids 39: 933–947

Kedishvili NY, Popov KM, Rougraff PM, Zhao Y, Crabb DW, Harris RA (1992) CoA-dependent methylmalonate-semialdehyde dehydrogenase, a unique member of the aldehyde dehydrogenase superfamily: cDNA cloning, evolutionary relationships, and tissue distribution. J Biol Chem 267: 19724–19729

Kleinboelting N, Huep G, Kloetgen A, Viehoever P, Weisshaar B (2012) GABI-Kat SimpleSearch: new features of the Arabidopsis thaliana T-DNA mutant database. Nucleic Acids Res 40: D1211–D1215

Klodmann J, Senkler M, Rode C, Braun HP (2011) Defining the protein complex proteome of plant mitochondria. Plant Physiol 157: 587–598

Lee P, Raj SM, Zhou S, Ashok S, Edwardraja S, Park S (2014) 3-Hydroxyisobutyrate dehydrogenase-I from Pseudomonas denitrificans ATCC 13867 degrades 3-hydroxypropionic acid. Biotechnol Bioprocess Eng 19: 1–7

Lokanath NK, Ohshima N, Takio K, Shiromizu I, Kuroishi C, Okazaki N, Kuramitsu S, Yokoyama S, Miyano M, Kunishima N (2005) Crystal structure of novel NADP-dependent 3-hydroxyisobutyrate dehydrogenase from Thermus thermophilus HB8. J Mol Biol 352: 905–917

Loupatty FJ, van der Steen A, Ijlst L, Ruiter JP, Ofman R, Baumgartner MR, Ballhausen D, Yamaguchi S, Duran M, Wanders RJ (2006) Clinical, biochemical, and molecular findings in three patients with 3-hydroxyisobutyric aciduria. Mol Genet Metab 87: 243–248

Mooney BP, Miernyk JA, Randall DD (2002) The complex fate of alpha-ketoacids. Annu Rev Plant Biol 53: 357–375

Morales A, Duque C (2002) Free and glycosidically bound volatiles in the mammee apple (Mammea americana) fruit. Eur Food Res Technol 215: 221–226

Murín R, Schaer A, Kowtharapu BS, Verleysdonk S, Hamprecht B (2008) Expression of 3-hydroxyisobutyrate dehydrogenase in cultured neural cells. J Neurochem 105: 1176–1186

Neuhoff V, Arold N, Taube D, Ehrhardt W (1988) Improved staining of proteins in polyacrylamide gels including isoelectric focusing gels with clear background at nanogram sensitivity using Coomassie Brilliant Blue G-250 and R-250. Electrophoresis 9: 255–262

Park SC, Kim PH, Lee GS, Kang SG, Ko HJ, Yoon SI (2016) Structural and biochemical characterization of the Bacillus cereus 3-hydroxyisobutyrate dehydrogenase. Biochem Biophys Res Commun 474: 522–527

Rasmusson AG, Soole KL, Elthon TE (2004) Alternative NAD(P)H dehydrogenases of plant mitochondria. Annu Rev Plant Biol 55: 23–39

Robinson WG, Coon MJ (1957) The purification and properties of beta-hydroxyisobutyric dehydrogenase. J Biol Chem 225: 511–521

Rougraff PM, Paxton R, Kuntz MJ, Crabb DW, Harris RA (1988) Purification and characterization of 3-hydroxyisobutyrate dehydrogenase from rabbit liver. J Biol Chem 263: 327–331

Schertl P (2015) Mitochondrial dehydrogenases in Arabidopsis thaliana. PhD thesis. Leibniz Universität Hannover, Hannover, Germany

Schertl P, Braun HP (2014) Respiratory electron transfer pathways in plant mitochondria. Front Plant Sci 5: 163

Senkler J, Senkler M, Eubel H, Hildebrandt T, Lengwenus C, Schertl P, Schwarzländer M, Wagner S, Wittig I, Braun HP (2017) The mitochondrial complexome of Arabidopsis thaliana. Plant J 89: 1079–1092

Shahmuradov IA, Umarov RK, Solovyev VV (2017) TSSPlant: a new tool for prediction of plant Pol II promoters. Nucleic Acids Res 45: e65

Shen J, Zeng Y, Zhuang X, Sun L, Yao X, Pimpl P, Jiang L (2013) Organelle pH in the Arabidopsis endomembrane system. Mol Plant 6: 1419–1437

Szabados L, Savouré A (2010) Proline: a multifunctional amino acid. Trends Plant Sci 15: 89–97

Tasi YC, Chao HC, Chung CL, Liu XY, Lin YM, Liao PC, Pan HA, Chiang HS, Kuo PL, Lin YH (2013) Characterization of 3-hydroxyisobutyrate dehydrogenase, HIBADH, as a sperm-motility marker. J Assist Reprod Genet 30: 505–512

Taylor NL, Heazlewood JL, Millar AH (2011) The Arabidopsis thaliana 2-D gel mitochondrial proteome: refining the value of reference maps for assessing protein abundance, contaminants and post-translational modifications. Proteomics 11: 1720–1733

Yamada K, Lim J, Dale JM, Chen H, Shinn P, Palm CJ, Southwick AM, Wu HC, Kim C, Nguyen M, et al (2003) Empirical analysis of transcriptional activity in the Arabidopsis genome. Science 302: 842–846

Yao T, Xu L, Ying H, Huang H, Yan M (2010) The catalytic property of 3-hydroxyisobutyrate dehydrogenase from Bacillus cereus on 3-hydroxypropionate. Appl Biochem Biotechnol 160: 694–703

Zhao J, Williams CC, Last RL (1998) Induction of Arabidopsis tryptophan pathway enzymes and camalexin by amino acid starvation, oxidative stress, and an abiotic elicitor. Plant Cell 10: 359–370